Composites & nanocomposites

Transverse viscoelastic properties of pulp fibers investigated with an atomic force microscopy method

Caterina Czibula[1,3] , Christian Ganser[1,3] , Tristan Seidlhofer[2,3] , Christian Teichert[1,3,*] , and Ulrich Hirn[2,3]

[1] *Institute of Physics, Montanuniversitaet Leoben, Franz Josef Str. 18, 8700 Leoben, Austria*
[2] *Institute of Paper, Pulp and Fiber Technology, Graz University of Technology, Inffeldgasse 23, 8010 Graz, Austria*
[3] *Christian Doppler Laboratory for Fiber Swelling and Paper Performance, Graz University of Technology, Inffeldgasse 23, 8010 Graz, Austria*

ABSTRACT

Changes in moisture content of single pulp fibers have an immense influence on the behavior of paper and paper products. Here, an atomic force microscopy (AFM)-based method is applied to investigate the viscoelastic properties of pulp fibers at varying relative humidity (RH) in the transverse direction. Pulp fibers have not only anisotropic properties, but also a very rough surface due to their hierarchical structure. For this reason, we have developed a specific load schedule for the AFM-based test method to overcome uncertainties and limitations due to surface roughness of the pulp fibers. The evaluation of the experimental data combines contact mechanics and viscoelastic models which consist of springs and dashpots in series or parallel describing elastic and viscous behavior. Here, it will be demonstrated that the so-called Generalized Maxwell (GM) model yields comparable results for single pulp fibers at five different RH values and in water. The moisture changes lead to a decrease in the elastic modulus but increase in the relaxation effects with increasing RH. All the determined parameters for the elastic and viscous behavior exhibit a gradual decrease with increasing RH from 10 to 75% RH. The elastic moduli decrease by a factor of 10 and the viscosities are decreasing by a factor of 10–20. In water, there is an even more pronounced decrease of the elastic moduli by a factor 100, and the viscosities decrease by at least three orders of magnitude compared to 10% RH. This indicates that the mechanical response of pulp fibers in water is significantly different than in humid air. This is also illustrated by the fact that a GM model of order two suffices to describe the material behavior in humid air but a GM model of order three is necessary to fit the material behavior in water. A possible interpretation is an additional relaxation effect of the pulp fiber wall in water.

Address correspondence to E-mail: teichert@unileoben.ac.at

Introduction

During paper making and processing, the mechanical properties of pulp fibers are strongly influenced by varying production and processing speeds and moisture. It is well known that pulp fibers are hygroscopic, and the interaction with water is crucial for the mechanical properties and ultimately for paper applications. Therefore, it is clearly beneficial to investigate the viscoelastic properties of pulp fibers at varying relative humidity (RH). Investigation of single pulp or even wood fibers is not straightforward, especially in transverse direction [1]. This is one reason why information on mechanical properties in the transverse direction is scarce. The lack of data also hinders the development of reliable models in transverse direction [2]. Another complication is the large variability of the material itself. The cell wall of a wood fiber is composed of a matrix of amorphous material which is surrounded by fibrils and consists of different layers (primary, S1, S2 and S3 layer) [3] which differ in thickness, chemical composition and fibril alignment. The S2 layer is the thickest and dominates the mechanical properties of the fiber [4]. Compared to the S2 layer, the S1 and S3 layers are much thinner, and during pulping the so-called primary layer usually gets removed due to its high lignin content and random fibril alignment.

For wood, attempts to describe viscoelastic behavior have been made on pine specimens along the grain [5] and on green wood in transverse direction [6]. The transverse mechanical properties of pulp and wood fibers have been investigated with different methods before. Earlier investigations of the transversal elastic modulus were based on lateral compression of wet fibers [7–9]. Also, tensile testing in an Environmental Scanning Electron Microscope (ESEM) utilizing image analysis has been developed for radial double-wall cut wood strips [10]. More recently, atomic force microscopy (AFM) [11] methods have proven to be very useful. AFM makes it possible to access the fiber surface on the nanoscale. Although it is most often used for the characterization of the morphology [12–14], the AFM probe can also be used as a force sensor. This way, a wide range of single fiber properties have been investigated like the flexibility [15] and conformability [16] of wet fibers. The creep behavior of wet fiber surfaces of hardwood chemi–thermo–mechanical pulp and

softwood kraft pulp has been studied as well [17]. AFM-based nanoindentation (AFM-NI) [18, 19] has been applied to characterize the mechanical properties of pulp fibers under controlled humidity. The results of AFM experiments can even help deepening the knowledge of fiber–fiber bonding [20] which is crucial for the understanding of paper performance [21]. In conclusion, viscoelasticity has been investigated for wood [5, 6], creep for hemp and pulp fibers has been studied only in longitudinal direction [22, 23]. In transverse fiber direction, however, only elastic properties have been studied [7–10].

To investigate viscoelasticity, two different experimental approaches are possible in general [24]. One option is dynamic measurements. Here, stress or strain is varied sinusoidally with time, and the response is measured at different frequencies. This approach has been used for, e.g., longitudinal viscoelastic properties of hemp fibers [22]. A dynamic AFM approach operating in a frequency range of 10 kHz to 1 MHz is contact resonance AFM (CR-AFM). Here, the change in the resonance curve between the free oscillation and during contact with the sample surface can be used to determine the viscoelastic properties semi-quantitatively. For the characterization of wood cells, CR-AFM has been applied, and it was observed that the obtained contact modulus yields lower values than nanoindentation [25].

Another approach to test viscoelasticity is a transient experiment. Here, the material is deformed, and the response is measured for a chosen time interval. If a constant strain is applied and the stress response is measured, the experiment is called stress relaxation. Keeping the stress constant and measuring the strain, on the other hand, corresponds to a creep compliance measurement. To locally characterize the viscoelastic properties dedicated AFM experiments, contact mechanics needs to be combined with a viscoelastic model. This has already been achieved in several ways. One straightforward possibility is to extract the time-dependent elastic modulus from a viscoelastic model and insert it in an arbitrary contact mechanics theory [26, 27]. Another approach is based on the simulation of the tip-sample contact [28–30].

In the present work, the creep compliance of single pulp fibers will be investigated employing contact mechanics in combination with an appropriate linear viscoelastic model. This method has been already successfully applied to the well-known polymers

polycarbonate and poly(methylmethacrylate) [31]. There, comprehensive validation of the method has been carried out by comparing the AFM-based measurement results to tensile testing and nanoindentation. Additionally, it was proven that the method can be applied to viscose fibers and provides values for the elastic properties which are comparable to AFM-NI results. Here, it will be demonstrated that a rather simple viscoelastic model is sufficient to obtain valid results in transverse fiber direction at different RH values for a hierarchically complex material like pulp fibers. During the experiment, the S1 layer surface is tested with our AFM-based method to obtain local creep curves. Afterward, we are employing a Generalized Maxwell (GM) model. The elastic behavior will be described by the parameters E_∞, E_1, E_2, and the viscous behavior will be characterized by the viscosities η_1 and η_2. Additionally, three auxiliary parameters can be defined, the two relaxation times, τ_1 and τ_2, and the instantaneous modulus E_0, which are helpful to interpret the relaxation behavior.

Methods and materials

Atomic force microscopy

All measurements in this work have been acquired with an Asylum Research MFP-3D AFM. The instrument is equipped with a closed-loop planar x–y-scanner with a scanning range of 85×85 μm^2 and a z-range of about 15 μm. Topography measurements were recorded in intermittent contact mode with standard silicon cantilevers (Olympus AC160-TS, Japan) with a nominal tip apex radius of about 10 nm and a nominal spring constant of 30 N m^{-1}. For the viscoelastic measurements, LRCH250 silicon probes (Team Nanotec, Germany) have been used. The spring constant of the cantilevers in use is (296 ± 46) N m^{-1} and has been calibrated by performing the thermal sweep method [32] (values are given as mean ± standard deviation calculated from 12 independent measurements). The thermal Q factor is 783 ± 160 and the resonance frequency is (593 ± 11) kHz. For measurements in water, the calibration of the LRCH250 probes was difficult due to the high stiffness of the cantilever. Therefore, a softer LRCH40 (Team Nanotec, Germany) probe was chosen instead. Again, the calibration of the spring constant was performed after [32]. The spring constant of this

cantilever is (70.8 ± 1.2) N m^{-1}, the thermal Q is 10.4 ± 0.08 and the resonance frequency is (209 ± 0.5) kHz (values are given as mean ± standard deviation calculated from 6 independent measurements).

Since the contact between tip and sample surface is crucial for mechanical characterization by AFM, the tip geometry of the probes was checked with a TGT01 (NT-MDT, Russia) calibration grid. Utilizing the tip-sample dilation principle [33], it is possible to image the AFM tip by scanning across a grid of sharp spikes. For the hemispherical LRCH250 and the LRCH40 probes, the tip radii were found to be (307 ± 21) nm and 345 nm, respectively. The main reason for using these probes with large tip radii was that the investigation of a larger surface area is possible. Additionally, higher forces can be applied with the indentation depths and strains remaining low. The strain should be small to claim linearity of the elastic and viscous response. This needs to be especially considered for investigating biological materials because they usually function at high strains and show nonlinear response [24, 34].

To investigate the pulp fibers in an environment with defined RH, the AFM was equipped with an Asylum Research closed fluid cell which can be controllably flushed by nitrogen.

The sensor to monitor RH and temperature (SHT21, Sensirion, Staefa, Switzerland) was placed directly inside the fluid cell, very close to the steel sample holder. This RH setup has been successfully employed before, and a more detailed description can be found in [18]. AFM measurements with samples immersed in distilled water were also conducted in a fluid cell to prevent damage of the AFM by leaking water. A water droplet with a diameter of about 10 mm covered the fibers completely and remained there for a whole day enabling long-time measurements.

For the measurement of mechanical properties with the AFM, the probe needs to get in contact with the surface. To achieve this contact, the AFM tip is approached to the surface with a velocity of 1 μm s^{-1} until a so-called trigger point of about 300 nN is reached. From this point onward, a force-indentation curve is recorded [35].

To determine the viscoelastic properties, the load schedule presented in Fig. 1 is applied. This is a modification of the load schedule which has been already presented and thoroughly discussed

Figure 1 Applied load schedule for the measurements at varying RH (solid line) and for the measurements in water (dashed line). The load schedule has two main parts. In part I, the fiber surface is plastically deformed and afterward relaxed for 300 s. In part II, a creep curve is recorded, and the viscoelastic response is tested. The icons **a**, **b** and **c** indicate the tip—sample interaction at different loads.
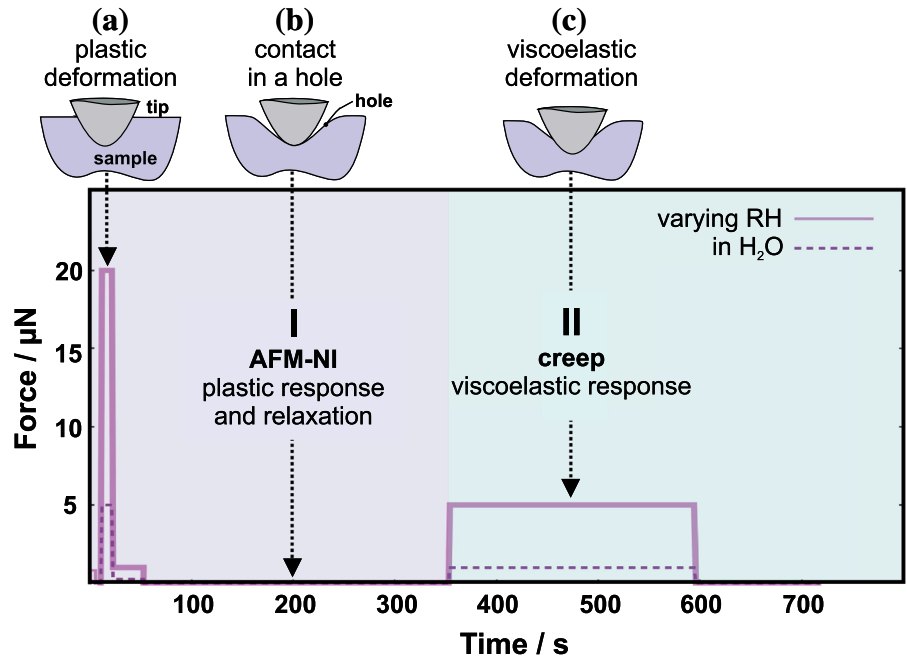
elsewhere [31]. Here, only the important points will be emphasized. The load schedule consists of two main parts (I, II) which will be explained in the following. In part I, a small load of 800 nN is applied to measure the initial indentation due to adhesion. Next, a high load of 20 μN is applied for 10 s to introduce plastic deformation to the sample surface (the interaction between tip and sample is indicated with icon (a) in Fig. 1). Here, also values for the reduced modulus E_r and hardness H according to the method of Oliver and Pharr [36] are obtained. Additionally, the plastic deformation makes it possible to characterize the contact between tip and sample surface in a more defined way. It is assumed that most of the local roughness is reduced due to this deformation and that the contact between tip and surface can be described as contact in a hole (icon (b) in Fig. 1). Due to the high load application, also further plastic response in part II is assumed to be eliminated.

After the plastic deformation, an unloading force of 1 μN is applied for 30 s. This is needed to account for viscoelastic effects and thermal drift in the AFM-NI evaluation. Then, only the trigger force is applied for 300 s to let the surface recover (icon (b) in Fig. 1). At the end of part I the surface has a well-defined shape due to the plastic deformation, as described in detail in [31]. The defined surface after plastic deformation can be used to model the viscoelastic response of the material in part II. There, a load of 5 μN with a loading rate of 3.2 μN s^{-1} is applied for 240 s, and the viscoelastic response or creep is measured (icon (c) in Fig. 1). The obtained creep curves are used for the evaluation of the viscoelastic properties.

With increasing RH value, the indentation depth for a fixed load of 5 μN increased in part II only slightly with δ_{max} (RH) = 0.6 nm %$^{-1}$, resulting in a maximum penetration depth of about 60 nm at 75% RH. However, measurement attempts of the fiber surfaces in water applying the same load schedule resulted in very high indentation depths (more than 1 μm). Due to that observation, the assumption that the surface is only elastically deformed during part II, could not hold anymore. For this reason, the load schedule was changed to lower force values. As indicated in Fig. 1, in part I only a load of 5 μN instead of 20 μN is applied, and in part II the load is adjusted to 1 μN. The load rates are identical.

Contact mechanics and adhesion

A contact mechanics model is required to relate the force and indentation depth measured in the experiment to the stress and strain in the viscoelastic model. The simplest model is based on the Hertz theory [37], which does not consider adhesion. When the AFM probe retracts from the sample surface, a negative force is needed to separate the tip from the surface.

This force is equivalent to the adhesion force and can be easily determined. Since it was found that adhesion during the experiments is between 100 and 900 nN, it cannot be neglected. For this reason, the Johnson–Kendall–Roberts (JKR) model [38], which does include adhesion, is the best option. It applies especially to the contact of a large radius probe with a soft sample surface [39]. Details on how the JKR and the viscoelastic model are combined and a study on the influence of adhesion is described in [31]. The fundamental equations of [31] which are used for the evaluation are outlined in the following: The definition of the equivalent loading force that accounts for adhesive effects F^* is,

$$F^*(t) = F(t) + 2F_{ad} + 2(F_{ad}F(t) + F_{ad}^2)^{1/2}, \qquad (1)$$

where $F(t)$ is the force applied during the experiment, and F_{ad} is the adhesion force. With this F^*, stress and strain can be obtained according to the JKR theory:

$$\sigma(t) = \frac{3F^*(t)}{8R\delta(t)} \left(1 - \frac{4}{3}\left(\frac{F_{ad}}{F^*(t)}\right)^{1/2}\right)^2, \qquad (2)$$

where $\delta(t)$ is the experimentally determined indentation depth and R is the effective radius of the contact between tip and surface.

Finally, the corresponding uniaxial strain equivalent is:

$$\varepsilon(t) = \frac{1}{2}\left(\frac{\delta(t)}{R}\right)^{1/2}\left(1 - \frac{4}{3}\left(\frac{F_{ad}}{F^*(t)}\right)^{1/2}\right)^{1/2}. \qquad (3)$$

This enables the stress–strain relation in the form of Hooke's law $\sigma = E\varepsilon$, commonly used in contact mechanics [40].

Viscoelastic models

Viscoelastic materials exhibit both, elastic and viscous characteristics when undergoing deformation and therefore, have a time-dependent behavior. There are different ways to describe viscoelastic material's response [24, 41]. One possibility would be the application of Prony series to describe the relaxation or creep time spectrum [42]. In this work, viscoelasticity is represented with linear differential equations. They arise from different combinations of Hookean elastic springs (denoted elastic moduli E_i) and Newtonian viscous dashpots (denoted viscosities η_i) describing elastic and viscous behavior,

respectively [43] (Fig. 2a, b). It is a useful tool to get an understanding of the complex material behavior at hand.

Viscoelastic models with only a spring and dashpot in series or parallel are too simple to establish a complex material model. On the other hand, models with too many parameters are difficult to interpret and make parameter identification challenging. Here, the Generalized Maxwell model of order two (GM2) proved to be appropriate and is presented in Fig. 2c. It consists of three springs (E_∞, E_1, E_2) and two dashpots (η_1, η_2). The combination of spring and dashpot in series (E_1 and η_1, E_2 and η_2) are so-called Maxwell elements. For each of these elements, it is possible to define a characteristic time, the relaxation time:

$$\tau_i = \frac{\eta_i}{E_i}, \qquad (4)$$

the ratio between viscosity η_i and elastic modulus E_i of the ith Maxwell element. In other words, the relaxation time is the time constant τ_i defining the restoring behavior of a Maxwell element, which
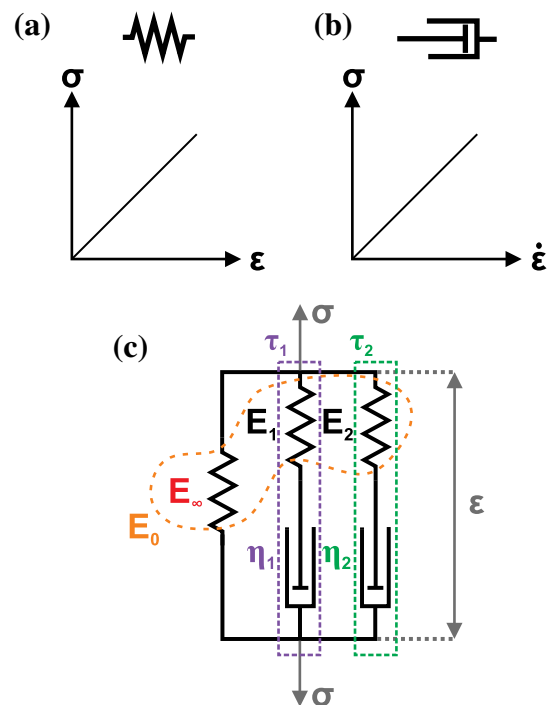

Figure 2 Viscoelastic models. a A Hookean spring represents linear elastic behavior, and b a Newton dashpot describes linear viscous behavior. In c, the Generalized Maxwell model of order 2 is depicted. It consists of three springs E_∞, E_1, E_2 and two dashpots η_1, η_2. Each dashpot is in series with a spring and forms a so-called Maxwell element.

relaxes proportionally to $e^{-\frac{t}{\tau_i}}$. Upon loading with a constant strain, the stress in a Maxwell element is decaying by the factor $1/e$ after the time τ_i has passed.

The GM2 model provides an upper and lower limit for the material's elastic modulus. If the loading is infinitely slow the strain rate $\dot{\varepsilon} \rightarrow 0$. This means only the infinite modulus E_∞ remains, E_1 and E_2 are zero. At infinitely fast loading, the dashpots become rigid, and only the springs deform leading to an instantaneous elastic modulus $E_0 = E_\infty + E_1 + E_2$.

The corresponding constitutive equation for the GM2 model is

$$\sigma = A\varepsilon + B\dot{\varepsilon} + C\ddot{\varepsilon} - D\dot{\sigma} - E\ddot{\sigma}, \tag{5}$$

with the coefficients $A = E_\infty$, $B = \left(\frac{E_1\tau_1 + E_2\tau_2}{E_\infty} + \tau_1 + \tau_2\right)E_\infty$, $C = \tau_1\tau_2(E_\infty + E_1 + E_2)$, $D = \tau_1 + \tau_2$, and $E = \tau_1\tau_2$ [31].

Since this is a differential equation of second order, two initial conditions need to be defined. One is the initial indentation δ_0. The force at the beginning is not zero, but equivalent to the applied trigger force, therefore, the tip is penetrating the surface by about 5–10 nm. The δ_0 values can be determined from the experiment [31]. Secondly, an initial indentation rate needs to be defined which is assumed to be zero.

Single fiber samples and preparation

The investigated single fiber samples were industrial, unbleached (Kappa value $\kappa = 42$; indicates the residual lignin content of the pulp), once dried and unrefined softwood kraft pulp fibers (Mondi Frantschach, Austria). These pulp fibers are a mixture of spruce and pine fibers with a length between 3 and 5 mm and a diameter of about 20–30 μm. The wood—used for the industrial pulp investigated here—contains both, trees from thinnings (juvenile wood) as well as sawmill chips (mature wood).

Fibers are wood cells with closed ends and so-called bordered pits which are cavities in the cell wall that provide liquid transport between individual cells. They are also essential for the identification of softwood species in pulp. Here, the geometrical form of the pits is important and can be identified for collapsed fibers with transmitted light microscopy. Spruce fibers are characterized with oval to round pits, while pine fibers show window-like, rectangular pits [44]. Measurements in this work have been performed on four spruce and two pine fibers. From the

shape and size of the pits, we think it is more likely that we have investigated earlywood fibers; however, this is uncertain. These fibers were all in the collapsed state. For the investigation of the mechanical properties with AFM, it is crucial that the fibers are fixed to a substrate and prevented from bending during load application. This is achieved by gluing the fiber with nail polish on a steel sample holder [20, 45]. Ideally, the fiber is embedded in the nail polish with only the surface of the fibers accessible for the measurements. Using this preparation procedure has proven to work for pulp fibers before [18].

To ensure that the fibers were tested in equilibrium moisture content, the sample was equilibrated overnight for at least eight hours at the desired relative humidity level. For measurements in water, the fibers were immersed in water for about 24 h before testing.

Outlier detection

The experimental data were examined with the Grubbs test [46], which tests normally distributed data for outliers. The test statistic g is obtained by:

$$g = \frac{|x_i - x_{\text{mean}}|}{s}, \tag{6}$$

where x_i is the ith measured value, x_{mean} is the mean and s is the standard deviation. The resulting g is compared to a table of critical values with significance level α of 0.01. If g is greater than the critical value, the corresponding value will be regarded as an outlier.

Results and discussion

Figure 3 shows an exemplary 5×5 μm^2 AFM image of a pulp fiber at 60% RH on which individual measurement points in smooth-looking regions were selected for the viscoelastic testing. The topography is presented before (Fig. 3a) and after (Fig. 3b) loading with the schedule presented in Fig. 1. As can be seen, the pulp fiber has a very rough surface which is dominated by wrinkle-like structures. Mostly the surface of the S1 layer has been investigated which was confirmed in earlier morphological studies with AFM [47]. In Fig. 3a, the diameter of the AFM probe, which is about 600 nm, is indicated by white dots. At the rather smooth positions of the dots, the viscoelastic testing experiment has been performed. Notably, the wrinkles on the pulp fiber surface are in
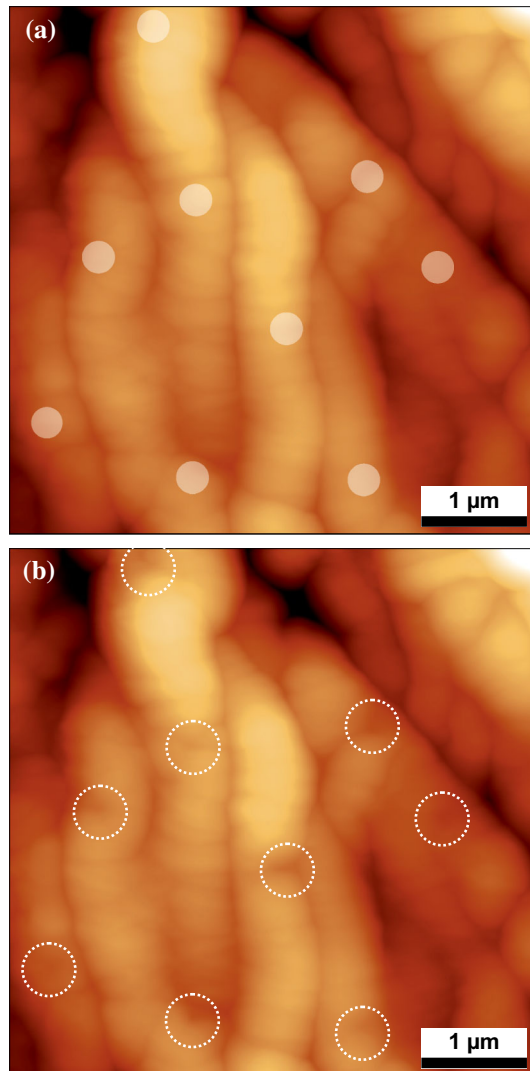
Figure 3 The effect of indentation visualized with AFM topography images. **a** AFM topography image (z-scale: 900 nm) before the viscoelastic testing experiment on a pulp fiber at 60% RH. The dots indicate measurement points, and the dot size corresponds to the diameter of the AFM tip. **b** AFM topography image (z-scale: 900 nm) of the same position after the experiment. The white dashed circles mark the holes from AFM-NI.

Altogether, six pulp fibers, four spruce and two pine fibers, have been investigated for their viscoelastic properties. Measurements have been obtained at 10%, 25%, 45%, 60% and 75% RH. Additionally, each fiber was measured while immersed in water.

Unfortunately, it was not possible to perform measurements at higher RH levels than 75% RH since condensation occurred in the AFM fluid cell during the long overnight equilibration and resulted in unstable measurement conditions. It should be noted that for the viscoelastic data evaluation of each measured region (corresponding to a $5 \times 5 \ \mu m^2$ window like in Fig. 3) an average curve of the individual measurement points (9 measurement points in Fig. 3b) has been calculated. The reason was to reduce the influence of thermal drift and signal noise, especially at lower RH, as described in more detail in [31].

For every fiber and each RH datapoint, at least three independent positions with at least eight individual measurement points per position should have been tested. These measurements are, however, not straightforward and subject to several factors of influence. First, pulp fibers show a high variability and sample preparation is difficult. The difficulties in sample preparation are mainly attributed to the fibers' geometry that hinders a firm and uniform contact with the nail polish embedding. Second, the selected AFM probes had a large tip radius that resulted in a low lateral resolution. It could not be assured that every measurement point was set on a sufficiently flat area. Third, the tip can become contaminated during measurements, which will influence the measurements by a change in contact area. This is often indicated by an increase in adhesion force due to the tip contamination. All these factors resulted that for every RH except 45% and 60% RH, measurements on only five individual fibers have been obtained. In detail, for 10% RH, 8 positions (44 indents), for 25% RH, 8 positions (61 indents), for 45% RH, 14 positions (123 indents), for 60% RH, 15 positions (117 indents), for 75% RH, 9 positions (64 indents) and in water, 17 positions (105 indents) have been obtained. At low RH, the fiber surface is so stiff that the AFM probe only penetrates a few nm. The signal–noise ratio is high even after averaging and, thus, the fitting quality was not good. At high RH and in water, some positions showed higher indentation depths and plastic deformation could not be

the same lateral size range as the diameter of the AFM tip. During measurement, lateral movement, e.g., bending, of these wrinkles cannot be excluded. However, it is assumed that most of this movement should take place during the plastic deformation. There, much higher loads are applied than during the viscoelastic testing. In Fig. 3b, the same pulp fiber surface is shown after the testing experiment. The white dashed circles indicate the permanent holes at the measurement positions, which have been formed during the AFM-NI part of the experiment.

fully ruled out even though in water the applied load was already lowered. Additionally, every fit that resulted in relaxation times outside the experimental window between the load time of 1.56 s (0.31 s in water) and 240 s was eliminated. This lower and upper limit was introduced to avoid misinterpretation of the relaxation behavior and only considering the experimental time scale.

In Fig. 4, representative experimental creep curves and the corresponding GM2 fits for all RH values are presented. As expected, the indentation depth and the initial slope of the experimental curves are increasing with increasing RH. The curves are fitted very well by the GM2 model. For more dynamic loading processes, the smaller time scale is very interesting, a closer look at the first 20 s of the measurements is provided in Fig. 4b. Also, in this range, the fits follow the experimental data very well, only at 75% RH the fit shows a slight initial deviation. The situation is different for fibers in water. A resulting creep curve for a measurement position in water with GM fits is presented separately in Fig. 5.

Figure 5a shows a representative experimental curve for a pulp fiber in water fitted with the GM2 model. In contrast to the data presented in Fig. 4, the indentation depth increased further, although according to Fig. 1, only 1 μN load has been applied during the creep experiment. As is clearly apparent in Fig. 5a, the GM2 approach is not fitting the data appropriately over the whole experimental time scale of 240 s. A possibility to improve the fitting is to add a third Maxwell element by using the Generalized Maxwell model of order three (GM3). To avoid too many fitting parameters and convergence problems, the values for the relaxation times were fixed for the evaluation procedure ($\tau_1 = 1$ s, $\tau_2 = 5$ s, $\tau_3 = 100$ s), and only the four parameters for the elastic moduli were fitted. (For the GM2 model, the fixation of the relaxation times to $\tau_1 = 5$ s and $\tau_2 = 100$ s, i.e., the mean values of the relaxation times at 75% RH, was also tried but was not successful.) After different
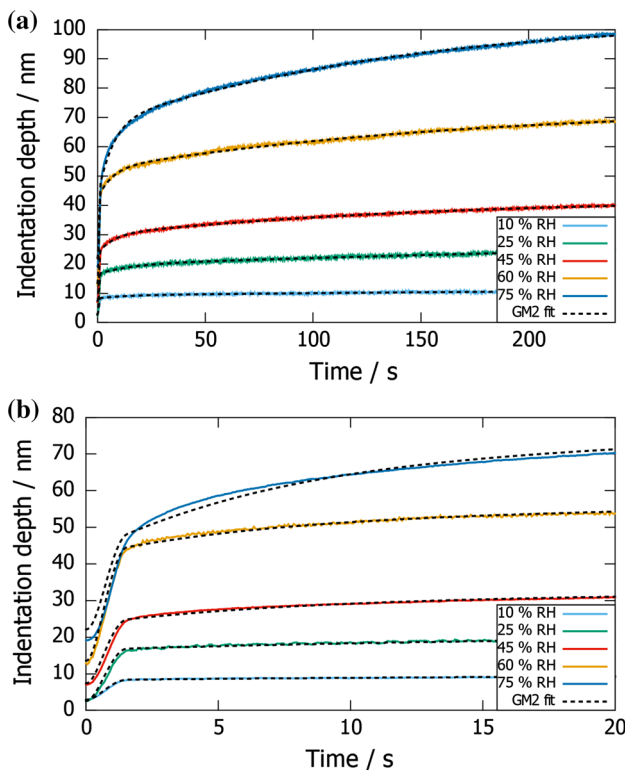

Figure 4 a Representative experimental creep curves at 10%, 25%, 45%, 60% and 75% RH with the corresponding fit curves as dashed lines. In b a closer look at the first 20 s of the experiment is provided.
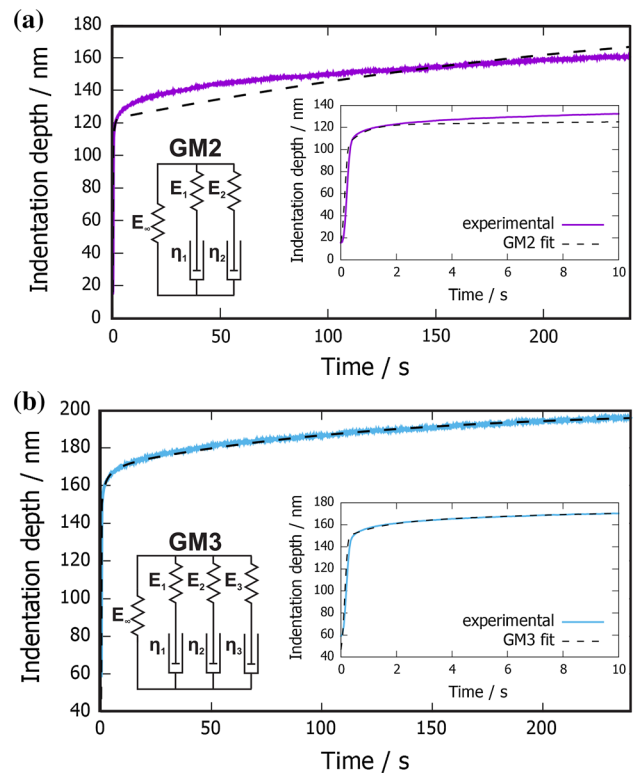

Figure 5 Comparison of the fits of the GM2 and the GM3 model for the same representative experimental curve of a measurement position under water. a Experimental creep curve (violet) with the GM2 fit as a black dashed line. In the inset, the first 10 s of the same experiment are presented. b Experimental creep curve (blue) with the GM3 fit as a black dashed line. In the inset, the first 10 s of the same experiment are presented.

fitting attempts, the most reasonable results were obtained by the introduction of a small relaxation time of $\tau_1 = 1$ s. In Fig. 5b, the same experimental curve as in Fig. 5a was fitted with the GM3 model. Overall, the fit shows little deviation and the GM3 model proves to be better suitable for the evaluation of the experimental curves in water. This indicates that an additional relaxation time is needed to describe the viscoelastic behavior in water accurately. Pulp fibers are porous, and in water the pores inside the cell wall are more likely to be filled up with water than pores of fibers in air. During penetration, the AFM tip might be displacing a water network and, thus, interfering with it [48]. Here, another approach could be using a poroelastic model to fit the data in water. It has been demonstrated that for nanoindentation experiments on hydrogels a poroelastic model showed superior fitting performance compared to a viscoelastic model [49].

In Fig. 6, the resulting viscoelastic properties and their dependence on relative humidity are presented. The presented results for all RH levels have been obtained from the GM2 model, only for the water measurements, the parameters of the GM3 instead of the GM2 model are indicated. No significant difference was detected between spruce and pine pulp fibers. Hence, the results from both fiber types were combined. The values presented in the diagrams are mean values obtained from six fibers. The corresponding values for each RH are also presented in Table 1. For water, the values of the GM2 and the GM3 model are compared in Table 2.

In Fig. 6a, the elastic moduli E_∞, E_1, E_2 and E_0 are presented. Since the water measurements have been evaluated with a GM3 model, an additional elastic modulus E_3 is introduced for the H$_2$O data. In general, the elastic parameters show a continuous decrease over the whole RH range. From 10% RH to 75% RH, the decrease is by a factor of 10. In water, however, the values drop by about three orders of magnitude compared to 10% RH. This jump-like decrease was already found for the reduced modulus and the hardness of pulp fibers with AFM-NI [18, 50]. It is generally known that the behavior of pulp fibers under water is different than for varying RH, but the mechanisms at work are still not clear. Immersed in water, the elastic moduli drop by a factor of 1000. Here, the values for E_3 are comparable to hydrogels like agarose and alginate [51, 52]. Cellulose is known to form hydrogels as well [53]. These gels have
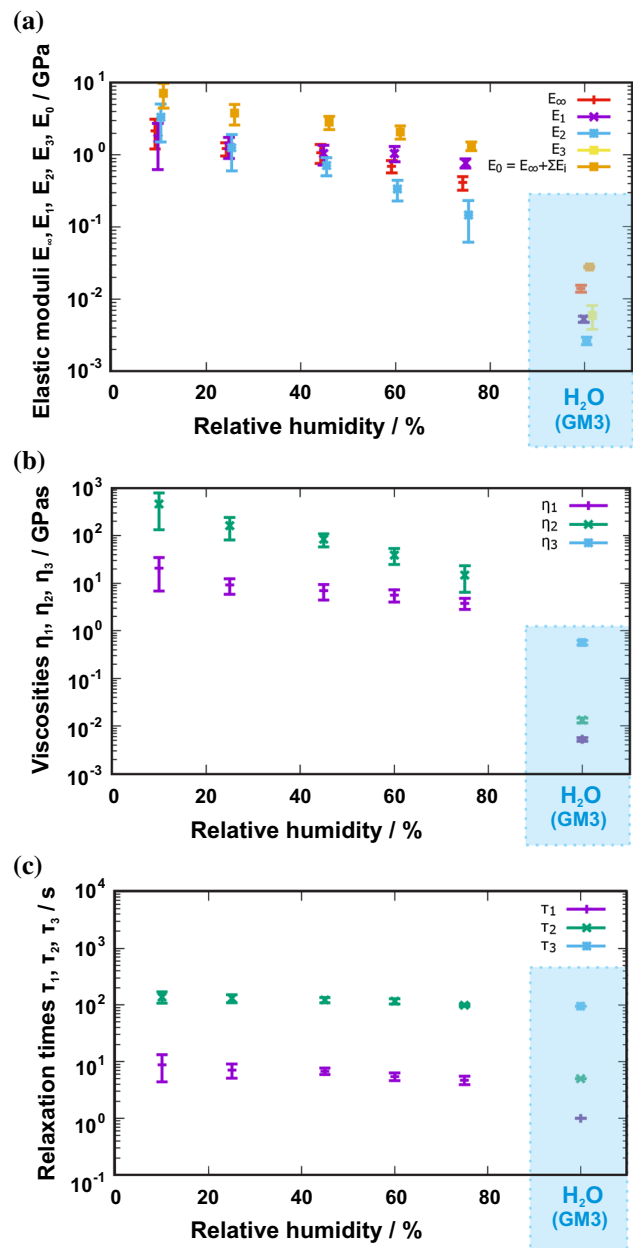

Figure 6 Semilogarithmic plots showing the RH-dependence of a elastic moduli E_∞, E_1, E_2 and E_0, b viscosities η_1 and η_2, and c relaxation times τ_1 and τ_2 of the GM2 model for 6 different pulp fibers. The mean values are plotted with the corresponding confidence intervals of 95%. For the GM3 fit of the water measurements, E_3, η_3 and τ_3 are also included.

shown a similar behavior in terms of relaxation behavior [54] and elastic modulus [55] like we have found in the current study. Recent molecular dynamics simulation of the S2 layer of wood fibers also suggest the formation of a water network at high moisture content [48].

Table 1 Results for the viscoelastic properties evaluated with the GM2 model

Relative humidity RH/%	E_∞/GPa	E_1/GPa	E_2/GPa	E_0/GPa	η_1/GPa s	η_2/GPa s	τ_1/s	τ_2/s
10% RH	2.2 ± 0.96	1.7 ± 1.05	3.3 ± 1.80	7.2 ± 2.71	21 ± 14	457 ± 325	9 ± 4	138 ± 31
25% RH	1.2 ± 0.26	1.3 ± 0.42	1.3 ± 0.65	3.8 ± 1.19	9 ± 3	160 ± 80	7 ± 2	130 ± 21
45% RH	1.1 ± 0.31	1.0 ± 0.31	0.7 ± 0.20	2.8 ± 0.59	7 ± 3	84 ± 26	7 ± 1	122 ± 13
60% RH	0.7 ± 0.14	1.1 ± 0.25	0.3 ± 0.11	2.1 ± 0.43	5 ± 2	36 ± 14	5 ± 1	116 ± 13
75% RH	0.4 ± 0.09	0.8 ± 0.11	0.1 ± 0.09	1.3 ± 0.18	4 ± 1	15 ± 8	5 ± 1	99 ± 6

The values are given as mean ± confidence interval of 95% obtained from 8 positions (44 indents) for 10% RH, 8 positions (61 indents) for 25% RH, 14 positions (123 indents) for 45% RH, 15 positions (117 indents) for 60% RH and 9 positions (64 indents) for 75% RH

Figure 6b presents the data for the viscosities at each RH. The behavior of the viscosities η_1 and η_2 with increasing RH is similar to that of the elastic moduli. Until 75% RH, the viscosities are decreasing by a factor of 10–20. Again, the—by far—lowest viscosities are observed when immersed in water. Here, the results for the three viscosity parameters η_1, η_2, and η_3 of the GM3 model in water decrease by 3 to 4 orders of magnitude compared to 10% RH.

In Fig. 6c, the relaxation times τ_1, τ_2 and, for water, τ_3 are presented. They show a rather steady behavior between 10% RH and 75% RH. There is a slight decrease by a factor of about 2, but it is not as pronounced as for the elastic moduli and viscosities. Equation 4 states that the relaxation time is defined as the ratio of viscosity and elastic modulus. For the GM2 model, between 10% RH and 75% RH, the elastic moduli E_1, E_2 and the viscosities η_1, η_2 decrease similarly, thus the ratio remains quite constant. As discussed earlier with respect to Fig. 6, the behavior in water is different, and a further Maxwell element is needed to fit the experimental data properly. With the introduction of an additional relaxation time τ_1 fixed at 1 s and τ_2 and τ_3 at 5 s and 100 s, respectively, the results for the elastic moduli and viscosities show less scattering and seem more reasonable. On the one hand, this effect could result just from an accelerated relaxation of the material in water. On the other hand, this could indicate an additional relaxation mechanism of the water saturated fiber wall that cannot be found in the investigated humidity range between 10% and 75% RH. If in water, the surface of the pulp fiber behaves more gel-like, the effect of migration of the water molecules underneath the indenter must be considered. This process is described by poroelastic deformation, and a poroelasticity approach would be needed to characterize hydrated cellulose networks [54]. However, such measurement would require a significant change in the experimental approach, which would go beyond the scope of this study.

Tables 1 and 2 list the results of the viscoelastic evaluation for the elastic (E_∞, E_1, E_2, E_3, E_0) and viscous (η_1, η_2, η_3) parameters as well as the relaxation times (τ_1, τ_2, τ_3) for all RH and water data points. In Table 3, the values for reduced modulus E_r and hardness H obtained from the AFM-NI part of the load schedule (see Fig. 1, part I) of each RH and water data point are presented. Using AFM-based nanoindentation, the E_r values in Table 3 are directly measured from the unloading slope of the force-distance curve after plastic indentation [19, 36], which is a totally different approach than fitting viscoelastic spring-dashpot models to the time response after indentation in the non-plastic regime like in Tables 1 and 2. Comparison of the results for E_0 at different RH and in water (Tables 1, 2) with the corresponding reduced modulus E_r values obtained from AFM-NI (Table 3) reveals that the values are in the same range. Moreover, the results of E_r and H obtained from AFM-NI show the same decreasing trend with increasing RH. This can be considered as an additional validation of the novel viscoelastic evaluation for pulp fibers presented here. For a detailed comparison of our elastic results to values for the transverse elastic modulus measured with other experimental techniques in the literature, please refer to the electronic supplementary information. The values in the literature show a high variation, which indicates the experimental difficulties associated with measurements in transverse fiber direction. In summary, the values for the elastic modulus obtained from the viscoelastic AFM-based method in this work are on the lower end, but still in the range of the existing literature.

Table 2 Results for the viscoelastic properties in water evaluated with the GM2 and GM3 model

H$_2$O	E$_\infty$/GPa	E$_1$/GPa	E$_2$/GPa	E$_3$/GPa	E$_0$/GPa	η$_1$/GPa s	η$_2$/GPa s	η$_3$/GPa s	τ$_1$/s	τ$_2$/s	τ$_3$/s
GM2	0.02 ± 0.004	0.02 ± 0.005	(7 ± 9)×10^{-4}	–	0.04 ± 0.009	0.03 ± 0.01	0.06 ± 0.09	–	1.2 ± 0.4	154 ± 36	–
GM3	0.01 ± 0.002	0.005 ± 3×10^{-4}	0.003 ± ×10^{-4}	0.006 ± 6×10^{-4}	0.03 ± 0.002	0.005 ± 5×10^{-4}	0.01 ± 0.002	0.56 ± 0.06	1	5	100

The values are given as mean ± confidence interval of 95% obtained from 7 positions (38 indents) for the GM2 model and 17 positions (105 indents) for the GM3 model in water

Table 3 Results for the reduced modulus E_r and hardness H obtained from AFM-NI

Relative humidity RH/ %	E_r/GPa	H/MPa
10% RH	6.3 ± 2.02	388 ± 71
25% RH	3.9 ± 1.15	327 ± 58
45% RH	2.2 ± 0.39	204 ± 35
60% RH	1.4 ± 0.25	146 ± 22
75% RH	0.9 ± 0.17	85 ± 21
H$_2$O	0.07 ± 0.01	8 ± 2

The values are given as mean ± confidence interval of 95% obtained from 8 positions (44 indents) for 10% RH, 8 positions (61 indents) for 25% RH, 14 positions (123 indents) for 45% RH, 15 positions (117 indents) for 60% RH, 9 positions (64 indents) for 75% RH and 17 positions (105 indents) in water

Conclusions

An atomic force microscopy-based method has been applied to investigate the viscoelastic properties of pulp fibers in transverse direction. This method has been successfully validated by the investigation of well-known polymers like polycarbonate and poly(methylmethacrylate) earlier [31]. In the present work, combining contact mechanics with the viscoelastic GM2 model allowed to measure creep on pulp fibers very locally and in transversal direction. Measurements have been carried out at different RH, ranging from 10% RH to 75% RH, and in water. The parameters from the GM2 model provide a good quantitative description of the transversal viscoelastic behavior at different moisture content. All the results for the parameters of the elastic and viscous behavior show a gradual decrease with increasing RH until 75% RH. From 10% RH to 75% RH, the elastic moduli decrease by a factor of 10. Until 75% RH, also the viscosities are decreasing by a factor of 10–20. Compared to that decrease, the relaxation times show a rather steady behavior between 10% RH and 75% RH.

For fibers immersed in water, the decrease is even more pronounced. The values for the elastic moduli drop by a factor 1000 and the viscosities show a decrease in at least three orders of magnitude compared to 10% RH. This indicates that the mechanical behavior and, therefore, the interaction between pulp fibers and water is different in water than at lower RH up to 75% RH. One explanation would be an additional relaxation mechanism, which corresponds to introducing a third Maxwell element to form a GM3 model. Also, other effects like poroelasticity

should play an increasingly dominating role in water because pulp fibers in the wet swollen state are known to form a cellulose hydrogel-like structure [56, 57] and the faster relaxation of the material in water could be related to the displacement of water from the pores due to the pressure of the indentation. Comparing the data with the AFM nanoindentation results, which have been also obtained from the experiments, the values for the elastic modulus E_0 from the viscoelastic GM models are in good agreement with the reduced modulus E_r from nanoindentation measurements.

Since the method works well for pulp fiber surfaces, the investigation of the S2 fiber wall layer will be the next step. The wood cell wall is divided into different cell wall layers, with the S2 layer being the thickest one. It also has the highest content of cellulose microfibrils, which are aligned very close to the direction of the fiber axis. Therefore, it is the layer which predominately influences mechanical properties, especially in longitudinal fiber direction [3, 48]. Here, the samples will be prepared from embedded microtome cuts. The goal will be to investigate the viscoelastic properties of the S2 layer of pulp fibers with the presented AFM-based method under the influence of RH and water.

Acknowledgements

Compliance with ethical standards

Conflict of interest We declare that no conflict of interest exists.

Electronic supplementary material: The online version of this article (https://doi.org/10.1007/s108 53-019-03707-1) contains supplementary material, which is available to authorized users.

References

[1] Eder M, Arnould O, Dunlop JWC et al (2013) Experimental micromechanical characterisation of wood cell walls. Wood Sci Technol 47:163–182. https://doi.org/10.1007/s00226-012-0515-6

[2] Bergander A, Salmén L (2002) Cell wall properties and their effects on the mechanical properties of fibers. J Mater Sci 37:151–156. https://doi.org/10.1023/A:1013115925679

[3] Salmén L (2018) Wood cell wall structure and organisation in relation to mechanics. In: Geitmann A, Gril J (eds) Plant biomechanics. Springer, Cham, pp 3–19

[4] Niskanen K (2008) Paper physics. Finnish Paper Engineer's Association/Paperi ja Puu Oy

[5] Penneru AP, Jayaraman K, Bhattacharyya D (2006) Viscoelastic behaviour of solid wood under compressive loading. Holzforschung 60:294–298. https://doi.org/10.1515/HF.2006.047

[6] Bardet S, Gril J (2002) Modelling the transverse viscoelasticity of green wood using a combination of two parabolic elements. C R Mec 330:549–556. https://doi.org/10.1016/S1631-0721(02)01503-6

[7] Hartler N, Nyrén J (1970) Transverse compressibility of pulp fibers. 2. Influence of cooking method, yield, beating, and drying. Tappi 53:820–823

[8] Wild P, Omholt I, Steinke D, Schuetze A (2005) Experimental characterization of the behaviour of wet single wood-pulp fibres under transverse compression. J Pulp Pap Sci 31:116–120

[9] Dunford J, Wild P (2002) Cyclic transverse compression of single wood-pulp fibres. J Pulp Pap Sci 28:136–141

[10] Bergander A, Salmén L (2000) The transverse elastic modulus of the native wood fibre wall. J Pulp Pap Sci 26:234–238

[11] Binnig G, Quate CF, Gerber C (1986) Atomic force microscope. Phys Rev Lett 56:930. https://doi.org/10.1103/PhysRevLett.56.930

[12] Fahlén J, Salmén L (2005) Pore and matrix distribution in the fiber wall revealed by atomic force microscopy and image analysis. Biomacromol 6:433–438. https://doi.org/10.1021/bm040068x

[13] Chhabra N, Spelt J, Yip C, Kortschot M (2005) An investigation of pulp fibre surfaces by atomic force microscopy. J Pulp Pap Sci 31:52–56

[14] Schmied FJ, Teichert C, Kappel L et al (2012) Analysis of precipitated lignin on kraft pulp fibers using atomic force microscopy. Cellulose 19:1013–1021. https://doi.org/10.1007/s10570-012-9667-7

[15] Pettersson T, Hellwig J, Gustafsson P-J, Stenström S (2017) Measurement of the flexibility of wet cellulose fibres using atomic force microscopy. Cellulose 24:4139–4149. https://doi.org/10.1007/s10570-017-1407-6

[16] Nilsson B, Wagberg L, Gray D (2001) Conformability of wet pulp fibres at small length scales. In: Proc. 12th fundamental research symposium. Oxford, pp 211–224

[17] Yan D, Li K (2013) Conformability of wood fiber surface determined by AFM indentation. J Mater Sci 48:322–331. https://doi.org/10.1007/s10853-012-6749-8

[18] Ganser C, Hirn U, Rohm S et al (2014) AFM nanoindentation of pulp fibers and thin cellulose films at varying relative humidity. Holzforschung 68:53–60

[19] Ganser C, Teichert C (2017) AFM-based nanoindentation of cellulosic fibers. In: Tiwari A (ed) Applied nanoindentation in advanced materials. Wiley, Hoboken, pp 247–267

[20] Schmied FJ, Teichert C, Kappel L et al (2013) What holds paper together: nanometre scale exploration of bonding between paper fibres. Sci Rep 3:2432. https://doi.org/10.1038/srep02432

[21] Hirn U, Schennach R (2015) Comprehensive analysis of individual pulp fiber bonds quantifies the mechanisms of fiber bonding in paper. Sci Rep 5:10503. https://doi.org/10.1038/srep10503

[22] Cisse O, Placet V, Guicheret-Retel V et al (2015) Creep behaviour of single hemp fibres. Part I: viscoelastic properties and their scattering under constant climate. J Mater Sci 50:1996–2006. https://doi.org/10.1007/s10853-014-8767-1

[23] Navi P, Stanzl-Tschegg SE (2009) Fracture behaviour of wood and its composites. Symp A Q J Mod Foreign Lit 63:139–149

[24] Vincent J (2012) Structural biomaterials. Princeton University Press, Princeton

[25] Arnould O, Arinero R (2015) Towards a better understanding of wood cell wall characterisation with contact resonance atomic force microscopy. Compos Part A Appl Sci Manuf 74:69–76. https://doi.org/10.1016/j.compositesa.2015.03.026

[26] Chyasnavichyus M, Young SL, Geryak R, Tsukruk VV (2015) Probing elastic properties of soft materials with AFM: data analysis for different tip geometries. Polym (UK). https://doi.org/10.1016/j.polymer.2016.02.020

[27] Chyasnavichyus M, Young SL, Tsukruk VV (2015) Recent advances in micromechanical characterization of polymer, biomaterial, and cell surfaces with atomic force microscopy. Jpn J Appl Phys 54:08LA02. https://doi.org/10.7567/JJAP.54.08LA02

[28] López-Guerra EA, Solares SD (2014) Modeling viscoelasticity through spring–dashpot models in intermittent-contact atomic force microscopy. Beilstein J Nanotechnol 5:2149–2163. https://doi.org/10.3762/bjnano.5.224

[29] Solares SD (2016) Nanoscale effects in the characterization of viscoelastic materials with atomic force microscopy: coupling of a quasi-three-dimensional standard linear solid model with in-plane surface interactions. Beilstein J Nanotechnol 7:554–571. https://doi.org/10.3762/bjnano.7.49

[30] Solares SD (2015) A simple and efficient quasi 3-dimensional viscoelastic model and software for simulation of tapping-mode atomic force microscopy. Beilstein J Nanotechnol 6:2233–2241. https://doi.org/10.3762/bjnano.6.229

[31] Ganser C, Czibula C, Tscharnuter D et al (2018) Combining adhesive contact mechanics with a viscoelastic material model to probe local material properties by AFM. Soft Matter 14:140–150. https://doi.org/10.1039/c7sm02057k

[32] Hutter JL, Bechhoefer J (1993) Calibration of atomic-force microscopy tips. Rev Sci Instrum 64:1868

[33] Villarrubia JS (1994) Morphological estimation of tip geometry for scanned probe microscopy. Surf Sci 321:287–300

[34] Moeller G (2009) AFM nanoindentation of viscoelastic materials with large end-radius probes. J Polym Sci Part B Polym Phys 47:1573–1587. https://doi.org/10.1002/polb.21758

[35] Butt HJ, Cappella B, Kappl M (2005) Force measurements with the atomic force microscope: technique, interpretation and applications. Surf Sci Rep 59:1–152. https://doi.org/10.1016/j.surfrep.2005.08.003

[36] Oliver WC, Pharr GM (1992) An improved technique for determining hardness and elastic modulus using load and displacement sensing indentation experiments. J Mater Res 7:1564–1583

[37] Hertz H (1881) Ueber die Berührung fester elastischer Körper. J Reine Angew Math 92:156–171

[38] Johnson KL, Kendall K, Roberts AD (1971) Surface energy and the contact of elastic solids. Proc R Soc A Math Phys Eng Sci 324:301–313. https://doi.org/10.1098/rspa.1971.0141

[39] Klapetek P (2013) Quantitative data processing in scanning probe microscopy, 2nd edn. Elsevier, Amsterdam

[40] Pathak S, Kalidindi SR, Klemenz C, Orlovskaya N (2008) Analyzing indentation stress–strain response of LaGaO3 single crystals using spherical indenters. J Eur Ceram Soc 28:2213–2220. https://doi.org/10.1016/J.JEURCERAMSOC.2008.02.009

[41] Banks HT, Hu S, Kenz ZR (2011) A brief review of elasticity and viscoelasticity for solids. Adv Appl Math Mech 3:1–51. https://doi.org/10.4208/aamm.10-m1030

[42] Sorvari J, Malinen M (2007) On the direct estimation of creep and relaxation functions. Mech Time-Dep Mater 11:143–157. https://doi.org/10.1007/s11043-007-9038-1

[43] Flügge W (1975) Viscoelasticity. Springer, Berlin

[44] Ilvessalo-Pfäffli M-S (1995) Fiber atlas. Identification of Papermaking Fibers, Springer, Berlin, Heidelberg

[45] Fischer WJ, Zankel A, Ganser C et al (2014) Imaging of the formerly bonded area of individual fibre to fibre joints with SEM and AFM. Cellulose 21:251–260. https://doi.org/10.1007/s10570-013-0107-0

[46] Grubbs FE (1969) Procedures for detecting outlying observations in samples. Technometrics 11:1–21. https://doi.org/10.1080/00401706.1969.10490657

[47] Ganser C (2011) Surface characterization of cellulose fibers by atomic force microscopy in liquid media and under ambient conditions. Montanuniversitaet, Leoben

[48] Kulasinski K, Derome D, Carmeliet J (2017) Impact of hydration on the micromechanical properties of the polymer composite structure of wood investigated with atomistic simulations. J Mech Phys Solids 103:221–235. https://doi.org/10.1016/j.jmps.2017.03.016

[49] Galli M, Comley KSC, Shean TAV, Oyen ML (2009) Viscoelastic and poroelastic mechanical characterization of hydrated gels. J Mater Res 24:973–979. https://doi.org/10.1557/jmr.2009.0129

[50] Persson BNJ, Ganser C, Schmied F et al (2013) Adhesion of cellulose fibers in paper. J Phys Condens Matter 25:045002. https://doi.org/10.1088/0953-8984/25/4/045002

[51] Li J, Illeperuma WRK, Suo Z, Vlassak JJ (2014) Hybrid hydrogels with extremely high stiffness and toughness. ACS Macro Lett 3:520–523. https://doi.org/10.1021/mz5002355

[52] Autumn K, Majidi C, Groff RE et al (2006) Effective elastic modulus of isolated gecko setal arrays. J Exp Biol 209:3558–3568. https://doi.org/10.1242/jeb.02469

[53] Kuga S (1980) The porous structure of cellulose gel regenerated from calcium thiocyanate solution. J Colloid Interface Sci 77:413–417. https://doi.org/10.1016/0021-9797(80)90311-2

[54] Lopez-Sanchez P, Rincon M, Wang D et al (2014) Micromechanics and poroelasticity of hydrated cellulose networks. Biomacromol 15:2274–2284. https://doi.org/10.1021/bm500405h

[55] Isobe N, Kimura S, Wada M, Deguchi S (2018) Poroelasticity of cellulose hydrogel. J Taiwan Inst Chem Eng 92:118–122. https://doi.org/10.1016/j.jtice.2018.02.017

[56] Pelton R (1993) A model of the external surface of wood pulp fibers. Nord Pulp Pap Res J 8:113–119

[57] Scallan AM, Grignon J (1979) The effect of cations on pulp and paper properties. Sven Papperstidn 2:40–47